USING GEOSTATISTICAL METHODS TO ESTIMATE SNOW WATER EQUIVALENCE DISTRIBUTION IN A MOUNTAIN WATERSHED

Benjamin Balk[1], Kelly Elder[2], Jill Baron[3]

ABSTRACT

Knowledge of the spatial distribution of snow water equivalence (SWE) is necessary to adequately forecast the volume and timing of snowmelt runoff. In April 1997, peak accumulation snow depth and density measurements were independently taken in the Loch Vale watershed (6.6 km^2), Rocky Mountain National Park, Colorado. Geostatistics and classical statistics were used to estimate SWE distribution across the watershed. Snow depths were spatially distributed across the watershed through kriging interpolation methods which provide unbiased estimates that have minimum variances. Snow densities were spatially modeled through regression analysis. Combining the modeled depth and density with snow-covered area (SCA) produced an estimate of the spatial distribution of SWE. The kriged estimates of snow depth explained 37-68% of the observed variance in the measured depths. Steep slopes, variably strong winds, and complex energy balance in the watershed contribute to a large degree of heterogeneity in snow depth.

INTRODUCTION

Mountain basins provide natural water storage in the form of a snowpack. About 75% of streamflow in the western United States results from snowmelt runoff (Doesken and Judson, 1996). Water is the lifeline of this region as downstream users rely heavily on snowmelt for agricultural, municipal, industrial, and recreational purposes. However, tremendous difficulties are encountered when trying to accurately predict the volume and timing of this water supply. The steep and variable topography of alpine catchments leads to a large degree of heterogeneity in snowpack properties, particularly the snow depth and snow water equivalence (SWE). The distribution of SWE is one of the controlling factors in the timing of runoff as different areas of mountain basins may generate snowmelt more rapidly than others. Before snowmelt models can be efficiently applied to predict the volume and timing of the release of this water supply, methods need to be developed to better estimate the distribution of SWE over alpine basins.

There are many factors which contribute to the variation of snow water equivalence (SWE). These factors, including elevation, slope, aspect, vegetation type, surface roughness, and energy exchange, are exaggerated in alpine areas leading to a heterogeneous snowpack that changes over time (Elder et al., 1991). In areas with gentle terrain, studies of seasonal snow cover are manageable as the importance of elevation, slope, and aspect to snow distribution is greatly diminished. However, in regions of rugged alpine terrain, understanding the processes controlling the spatial distribution of snow is difficult.

Although the further development of remote sensing will greatly benefit the field of snow hydrology, the use of remote sensing alone to estimate basin-wide SWE for alpine watersheds is not yet fully operational. Although snow-covered area can be measured through aerial photography and satellite imagery, operational measurements of SWE in mountain environs are still ground-based (Elder et al., 1997). Therefore, interpolation between ground-based point measurements becomes necessary to explain and understand the spatial distribution of SWE over an entire drainage basin. Previous research efforts using intensive snow surveys (e.g., Elder et al., 1991 and 1997; Hosang and Dettwiler, 1991; Elder, 1995) have shown progress in distributing measured values of SWE over a region.

In this paper, we present a geostatistical method for estimating the spatial distribution of SWE in a mountain watershed in the Colorado Front Range.

[1]Department of Earth Resources, Colorado State University, Fort Collins, CO 80523, Tel: 970-249-6774, Email: bbalk@cnr.colostate.edu *or* cbalk@montrose.net

[2]Department of Earth Resources, Colorado State University, Fort Collins, CO 80523, Tel: 970-491-5454, Email: kelder@cnr.colostate.edu

[3]Natural Resource Ecology Laboratory, Colorado State University, Fort Collins, CO 80523, Tel: 970-491-1968, Email: jill@nrel.colostate.edu

Paper presented at the Western Snow Conference, Snowbird, Utah, April, 1998.

BACKGROUND

Geostatistics emerged in the early 1960's as a hybrid discipline of mining engineering, geology, mathematics, and statistics. Geostatistics evolved independently of the mainstream of statistics and its terminology retains a strong mining flavor. The discipline arose from the need to improve estimates of ore concentration and recoverable reserves from fragmentary information (Webster and Oliver, 1990). By modeling both spatial trend and spatial correlation, geostatistics offered a stronger approach to ore-reserve estimation than more classical approaches (Cressie, 1991). Geostatistical methods are applicable throughout the Earth sciences, especially the hydrologic sciences. Examples of such applications include the mapping and modeling of groundwater (cf., Gambolati and Volpi, 1979; Dunlap and Spinazola, 1984), estimation of mean annual precipitation (cf., Tabios and Salas, 1985; Phillips et al., 1992), and estimation of snow water equivalence (cf., Hosang and Dettwiler, 1991; Carroll and Cressie, 1996).

Natural phenomena can often be characterized by the distribution of one or more regionalized variables, which are essentially functions taking a definite value in each point in space (Matheron, 1963). Given the value of a variable at a point, one is concerned with the variability of the function as the variable changes in space. A representation of the variability, the variogram, can then be used to estimate the value $z(x_o)$ at a point x_o at which no data are available (Journel and Huijbregts, 1978). This interpolation method, known as kriging, consists of three steps: (1) examining the covariation of data values depending on their separation distance; (2) fitting theoretical models to these relationships; and (3) using these models to calculate the weights for a particular set of neighboring points and to compute the interpolated value (Phillips et al., 1992).

Experimental Variogram

The first step in the kriging interpolation method is constructing an experimental semivariogram, usually referred to as a 'variogram.' The variogram is a representation of the spatial variability of a regionalized variable that is randomly distributed in space, but shows the degree of continuity embedded within this randomness (Hosang and Dettwiler, 1991). To estimate the variogram for an observed spatial process, it is necessary in practice to assume some sort of stationarity for that process, i.e., a constant mean and constant variance throughout the study region (Bailey and Gatrell, 1995). All possible pairs of data points are examined and grouped by distance classes. One half the variance of the difference in values, the semivariance, is then graphed versus the distance class. Thus, the variogram can be graphed according to:

$$\gamma(h) = 1/2n \sum_{i=1}^{n} [z(x_i) - z(x_i + h)]^2 \qquad (1)$$

where $z(x_i)$, $z(x_i+h)$ are samples taken at locations x_i and x_i+h respectively, and n is the number of pairs separated by the vector **h** (Herzfeld et al., 1990). The vector **h** separates the two locations x and $x+h$ in both distance and direction. The ordered set of values obtained by increasing h constitutes the experimental variogram. Equation (1) indicates that the variance of $z(x)$ depends on the separation h and not on the actual position of x (Oliver et al., 1989). Having the same variance for a given distance, regardless of direction, is known as isotropy. Isotropic conditions are often assumed to obtain a description of variance structure which is sufficiently simple. However, directional differences, or anisotropy, should be tested for by estimating the variogram in various directions.

Fitting a Theoretical Model

The experimental variogram is estimated from discrete values of **h**, whereas the true variogram is continuous. Furthermore, the limited number of sample points will usually not allow for an accurate representation of the true variogram. Therefore, it is necessary to fit a theoretical model to the sample values to represent the true variogram. The theoretical model is characterized by parameters, which are the nugget effect, the sill, and the range (Figure 1). The nugget effect, or variance at zero distance, arises from a combination of measurement errors and spatially dependent variation on scales much shorter than the smallest sampling interval. The sill represents the *a priori* variance of the measurements and is the variance to which the variogram asymptotically rises. The range defines the limit of spatial dependence, i.e., the maximum distance over which interpolation is meaningful (Oliver et al., 1989).

The objective of variogram modeling is to capture the basic structure of spatial dependence. A theoretical model is fit to the sample data by least-squares regression, or by optimizing through cross-validation procedures. Three of the most commonly used variogram models, the spherical, exponential, and Gaussian, are explained in Bailey and Gatrell (1995). Many other theoretical models, both bounded by the sill variance and unbounded, are explained in detail by Journel and Huijbregts (1978) and Oliver et al. (1989).

Kriging

Once a theoretical model has been established, kriging interpolation can be performed. At its simplest, kriging is a method of weighted averaging of the observed values of a measurement space Z, within a neighborhood V, from the measured values $z(x_i)$ of Z at n sites, x_i, i=1,2,...,n (Oliver et al., 1989). To calculate an interpolation value, the weights of the neighboring measurement sites have to be determined by solving a system of equations that

consider the theoretical variogram model. For simple kriging, interpolations are made using only the variogram for the variable to be estimated. For cokriging, additional variograms for correlated variables and cross-variograms for their interactions are used (Phillips et al., 1992).

In contrast to all other interpolation schemes, kriging has the major advantage of offering the ability to calculate the estimation variances associated with the interpolated values. Further calculations involving the interpolated values are, therefore, possible with a determinable uncertainty (Hosang and Dettwiler, 1991). In addition, kriging is an exact interpolator, meaning a kriged surface will pass through measured values giving zero deviance at the sampled points.

STUDY SITE

Loch Vale watershed (LVWS) is located in Rocky Mountain National Park, Colorado, at 40° 17' N, 105° 40' W (Figure 2). This glacially scoured basin lies in the Front Range immediately east and below the Continental Divide with elevations between 3091 and 4003 m. The basin has a general east-northeast aspect and is flanked by steep cliffs on most margins. Slopes in LVWS range from a minimum of 0° to a maximum of 85° with the mean slope for the basin being 33°. The watershed has an area of approximately 6.6 km^2 and is drained by Andrews Creek and Icy Brook. Andrews Creek and Icy Brook eventually feed the Big Thompson River, a major tributary of the South Platte River. A more detailed description of the watershed can be found in Baron and Mast (1992).

FIELD METHODS

An extensive snow survey was completed in LVWS during 15-18 April, 1997. Snow depths were measured at 222 points, and snow densities were measured in seven snowpits (Figure 3). Sample locations were chosen to be representative of the range of elevations, slopes, and aspects of the watershed with safety constraints. The sample locations were then transcribed onto the USGS 7.5' McHenrys Peak Quadrangle. The respective UTM coordinates were obtained for each sampled site and were registered to a 10 m resolution digital elevation model (DEM) of LVWS.

The watershed was divided into three subbasins, Andrews Creek, Sky Pond, and Lower Loch (Figure 2), and maps of each subbasin were enlarged from the USGS 7.5' McHenrys Peak Quadrangle. Arbitrary grid systems were aligned with the valley walls of each subbasin. A 50 m grid was placed over the Andrews Creek and Sky Pond subbasins and a 100 m grid was established for the Lower Loch. The finer resolutions grids were established to obtain a higher concentration of sample points for the upper drainages of LVWS where the heterogeneity in snow depths was apparent.

Depth measurements were made with aluminum probe poles. At each sample point, three depth measurements were made (a central one plus two in directions aligned with the grid at 5 m spacing from the center). The three measurements were recorded to the nearest 0.05 m and averaged to minimize local variation in depth. In the upper drainages, only one measurement was made at most sample points and the sampling was shifted to 100 m spacing due to probing difficulties and time constraints. The spacing between grid points was measured using probe poles.

Seven snowpits were dug in the watershed to obtain density and temperature profiles. Density was measured with a 1-L stainless steel wedge-shaped cutter and an electronic digital scale with 1 g resolution and ±0.5 g accuracy. Continuous density profiles were sampled in 0.10 m increments, which were then averaged to obtain one representative density for each snowpit. Temperature profiles from the seven snowpits indicated the cold content had not been entirely removed as snowpack temperatures ranged from near 0°C to -9°C. There was no significant snowmelt in LVWS before the 15-18 April snow survey.

MODELING METHODS

Previous studies have determined a connection between some parameters and the processes controlling the distribution of snow. Radiative fluxes and physiographic features, such as elevation, slope, aspect, roughness, and the optical and thermal properties of the substrate, rationally and demonstrably relate to snow cover variations (McKay and Gray, 1981). In this statistical attempt at modeling SWE across LVWS, we used the independent variables of net solar radiation and elevation.

Net Solar Radiation

Net solar radiation has been shown to be the largest energy source for melting alpine snowpacks (Megehan et al., 1967; Zuzel and Cox, 1975). In addition to being the most important component in the energy balance for modeling snowmelt, net radiation also plays a controlling role in the accumulation and redistribution of snow. Elder (1995) found that using a spatially distributed net solar radiation index over a portion of the snow accumulation season may be sufficient for many applications, such as statistical efforts to model SWE distribution in alpine areas.

To model net solar radiation in LVWS, we used **ipw** (Image Processing Workbench) software (Frew and Dozier, 1986). The **ipw** program, **topquad**, integrates the solar radiation inputs over the course of a day to yield the total solar radiation loading. The information required for **topquad** to compute the spatial distribution of solar radiation includes a DEM, slope and aspect maps, sky view factor, terrain configuration factor, surface albedo map, and atmospheric parameters. The slope and aspect maps, along with the sky view and terrain configuration factors, can be derived from the DEM with **ipw**. Temporal variations of albedo throughout the accumulation season are too great to model absolutely, so we estimated albedo for the visible and near infrared wavelengths for each month between December and April (Wiscombe and Warren, 1980) assuming total basin snow cover. The atmospheric parameters required to run **topquad** can be derived from the model LOWTRAN7 (Kneizys et al., 1988).

Using the 10 m DEM for LVWS, net solar radiation was calculated, assuming clear-sky conditions, for all grid cells in the basin for the 15th of each month from December through April. These spatially distributed maps of daily net radiation were then summed to obtain one radiation image representing an index of net solar radiation through a portion of the snow accumulation season (Figure 4).

Elevation

Primarily through orographic effects, elevation has been shown to be an important factor in snow distribution (Rhea and Grant, 1974; Caine, 1975). For a small catchment in Switzerland's Jura Mountains, Hosang and Dettwiler (1991) found that elevation exerted the strongest influence on the distribution of SWE. In this study, elevations were obtained from the 10 m DEM constructed for LVWS (Figure 3). Vertical errors for the elevations are assumed to be less than 1 m (Cline, personal communication, 1997).

Snow Density

Snow density measurements involve excavating snowpits and sampling the snowpit wall. Snow depth measurements simply require probing and subsequently, are much less labor-intensive and time consuming. In alpine areas, the major source of variation in SWE is variation in depth, especially during the melt season (Logan, 1973; Elder et al., 1991). The conservative variation of density assists field sampling as a few density profiles can supplement many more easily obtained depth measurements. Although density is conservative in relation to other snow properties such as depth, it does exhibit some spatial variation (Elder, 1995). Thus, the measured densities need to be spatially distributed across LVWS.

Elevation and slope did not show a significant relationship with snow density; thus, only and index of net solar radiation was used as the independent variable when modeling density. A general linear model, which explained 53% of the observed variance in field measurements of snow density, was used to distribute density (R^2 = 0.529, n = 7, p = 0.064). This general linear model proved sufficient except for low radiation values which produced unrealistically low densities. Since the snowpits were generally located along the valley floors, the modeled radiation values for those locations were relatively high due to the combination of direct beam and reflected irradiance. Therefore, a binary regression tree (Breiman et al., 1984; Clark and Pregibon, 1992) was used to determine a representative lower limit radiation value. With snow depth as the dependent variable and net solar radiation as the independent variable, a regression tree was developed from the 222 sampled snow depth points using the S-Plus mathematical language (Chambers and Hastie, 1992). Snow depth, instead of density, was used as the dependent variable because in general terms, with greater depth we expect greater mean densities due to compaction and metamorphism. In addition, the number of density measurements (n = 7) was not sufficient to grow a regression tree. The regression tree was grown to see if any early splits would correlate with the radiation indices modeled at the density snowpits. An early split in the regression tree (where the radiation was less than 728 W m^{-2}) correlated well with the measured weighted mean densities. For all radiation values less than 728 W m^{-2}, a snow density of 300 kg m^{-3} was assigned. This density value was the lowest weighted mean density of the seven snowpits and was the only measured density with a radiation less than 728 W m^{-2}. Figure 5 shows the distributed density across LVWS.

Snow Depth

Geostatistical methods were used to model snow depth in LVWS. Using the S-Plus mathematical language (Chambers and Hastie, 1992), snow depths were spatially distributed across the watershed through kriging interpolation techniques. Three different snow depth models were developed: (1) kriging on the primary variable, snow depth; (2) cokriging using the auxiliary variable radiation to aid the estimates of snow depth; and (3) cokriging

using elevation as the auxiliary variable. Interpolations were made for each 10 m cell of the DEM in a procedure known as block kriging. Block kriging operates under the same principles as simple kriging described earlier, except the interpolated value is averaged over a block; in this case a 10 m cell.

For the three models, experimental variograms were constructed with maximum distance parameters and a certain number of distance classes, or bins, to best represent the spatial variability of snow depth. The means and variances of the regionalized variable were assumed to be independent of location and constant throughout the watershed. Since no significant directional differences in the experimental variograms were found, isotropic variance structure was also assumed. These experimental variograms were then fitted with Gaussian, spherical, exponential, and linear variogram models. These fitted theoretical models were weighted by the number of pairs found in each bin. The best-fit theoretical variograms used in the kriging interpolations were selected based on the highest coefficient of determination found through least-squares regression. The results of the variogram fitting procedure with the variograms for depth and the correlated variables and the cross-variograms for their interactions are given in Table 1.

Table 1. Variogram fitting results

Model	*Number of bins for experimental variogram*	*Theoretical model type*	*Coefficient of determination (R^2)*
Kriging			
-Depth variogram	25	Gaussian	0.890
Radiation Cokriging			
-Depth variogram	25	Gaussian	0.890
-Radiation variogram	20	Spherical	0.379
-Cross-variogram	15	Gaussian	0.173
Elevation Cokriging			
-Depth variogram	25	Gaussian	0.890
-Elevation variogram	10	Gaussian	0.976
-Cross-variogram	10	Gaussian	0.692

The Gaussian theoretical model was most frequently used in this study. The Gaussian model is described by:

$$\gamma(h) = c_o + c(1 - e^{3h^2/a^2}), \quad \text{for } h > 0 \qquad (2)$$

$$\gamma(h) = 0, \quad \text{for } h = 0$$

where a is the range, c is the sill variance, and c_o is the nugget effect. The experimental variogram and theoretical Gaussian model fit for the kriging model are shown in Figure 1.

Cross-validation was used to evaluate the statistical properties of the kriged surface and to determine the ideal number of nearest neighbors, or sampled depth measurements, to be used in each kriging model. Each sample depth point, x_i, was suppressed in turn, and its value was predicted from the remaining data using the selected variogram model. A measure of the overall goodness of fit of each kriging model can be assessed by the coefficient of determination (R^2). The coefficient of determination for each kriged surface was calculated from the measured depths and the kriged estimates of depth at each sample point.

Snow-Covered Area

Snow-covered area (SCA) for this study was determined using an aerial photograph of LVWS taken on 9 April, 1996. No aerial flight was made in 1997, but due to the extreme topography of LVWS, it is assumed that SCA near peak accumulation will be fairly consistent from year to year since most of the steeper slopes in the watershed cannot maintain snow cover, even during heavy snowfall years. The 9 April, 1996 aerial photograph was orthorectified to the 10 m DEM for the watershed. A binary threshold was then chosen to most accurately depict SCA for the orthoimage. The binary threshold was determined such that pixels with a digital number (DN) value less than the threshold were assigned a DN of 0 (black), and pixels with a DN value greater than the threshold were assigned a DN of 255 (white). This procedure did not distinguish forested and shaded areas from cliff bands that were snow free. Therefore, a mask of the forested and shaded areas that were snow-covered was created and combined with the binary threshold image to produce the final snow-covered image (Figure 6). The SCA for LVWS was calculated to be 56% of the watershed area.

RESULTS

Snow Depth

The validity of the kriging interpolations of snow depth was quantitatively examined through cross-validation. The differences between the measured and kriged estimates of depth, the residuals, were considered as well as the standard deviation of the estimates and the coefficient of determination for each model. These evaluations are summarized in Table 2.

Table 2. Evaluation of kriging interpolation models

Model	*Number of nearest neighbors*	*Mean of residuals (m)*	*Absolute value of the mean of residuals (m)*	*Mean standard deviation of estimates (m)*	*Coefficient of determination (R^2)*
Kriging	10	0.011	1.301	1.723	0.365
Radiation Cokriging	2	0.002	0.831	1.909	0.684
Elevation Cokriging	2	-0.012	0.828	1.919	0.684

The optimal number of nearest neighbors to be used in each kriging interpolation method was chosen from cross-validation runs (Figure 7). As is the case for all three models, the mean of the residuals should be centered around zero. The absolute values of the mean of the residuals indicate that the kriged estimates of depth from the cokriging models are closer in value to the measured depths. This characteristic of the residuals also is shown in the R^2 values, where the two cokriging models explain more of the observed variance (R^2 = 0.684) in the field measurements of depth than the kriging model (R^2 = 0.365). However, the means of the standard deviation of the estimates across the watershed show that the kriging model has the lower estimation errors.

Snow Water Equivalence

The snow water equivalence (SWE) distribution for each kriging model was calculated by multiplying the kriged depth surface by the modeled density and SCA map (Figure 8). All three models show relatively high SWE accumulations in the Andrews Creek subbasin and relatively low SWE accumulations in the Sky Pond subbasin. The Sky Pond subbasin is broader than the Andrews Creek subbasin, and subsequently receives more direct radiation (Figure 4). The greater radiation and typical strong winds are considered primary reasons behind the lower accumulations of SWE around Sky Pond. The effects of wind redistribution of snow can also be seen along the western margins of LVWS. These areas, just to the lee side of the Continental Divide, accumulate large amounts of SWE. The total SWE volumes for each kriging model are listed in Table 3.

Table 3. Snow water equivalence comparisons for kriging interpolation models

Model	*Mean SWE depth (m)*	*Total SWE volume (m^3)*
Kriging	0.63	4,400,000
Radiation Cokriging	0.65	4,500,000
Elevation Cokriging	0.66	4,600,000

DISCUSSION

The cokriging models for both radiation and elevation yield higher R^2 values than the kriging model. However, the R^2 values for the two cokriging models rapidly decrease when the number of nearest neighbors considered in the kriging interpolation increases. This phenomenon can possibly be the result of low spatial correlation between both radiation and elevation and the primary variable, snow depth. The radiation cokriging model has a negative R^2 when the number of nearest neighbors is greater than 12, while the elevation cokriging model has a negative R^2 when the number of nearest neighbors is greater than four. These negative R^2 values indicate that the variance of the residuals is greater than the variance of the observed snow depths, i.e., the kriged surface is less useful for modeling snow depth than the original surface. On the other hand, the R^2 values for the kriging model make more intuitive sense as they increase with increasing number of nearest neighbors (Figure 7).

Although the cokriging models have higher R^2 values, they only consider a small number of depth measurements (n = 2) in their interpolation process. This characteristic inhibits the ability to interpolate depths at distances far away from the sampled sites and explains the polygonal structure of the cokriged SWE maps (Figures 9 and 10). Cokriging may be advantageous in situations where the auxiliary variables are highly correlated with the primary variable ($|r| > 0.5$; $R^2 > 0.25$) (Phillips et al., 1992). However, radiation ($R^2 = 0.026$) and elevation ($R^2 = 0.059$) do not show high correlation with snow depth in this study. The lack of correlation between the auxiliary variables (radiation and elevation) and the primary variable (depth), along with the small number of nearest neighbors used in the interpolation process, indicate that the two cokriging models yield rather poor results despite explaining 68.4% of the variance in the measured snow depths.

The kriging model only explains 37% of the observed variance in the field measurements of snow depth ($R^2 = 0.365$). This R^2 value is somewhat low compared to previous studies incorporating kriging techniques. Promising results from kriging interpolation have been obtained (cf., Tabios and Salas, 1985; Phillips et al., 1992; Carroll and Cressie, 1996), but these studies dealt with larger spatial scales which tended to smooth the effects of topography and allowed for significant trends in the data to be found. We feel the extreme topography of the small LVWS plays the dominant role in this low R^2 value. Due to its location just below the Continental Divide, LVWS is subject to strong winds that are funneled by the glacial terrain. The rugged terrain forces these winds to have extremely complex patterns resulting in a mosaic of wind scour and depositional areas. The rugged terrain also leads to very heterogeneous radiation inputs across the watershed. The steep topography, variable winds, and uneven radiation balance are primary contributors to the large heterogeneity in snow depth found in LVWS. This large heterogeneity in snow depth complicated the kriging interpolation process.

CONCLUSION AND FUTURE WORK

Applying the geostatistical method known as kriging to improve estimates of SWE distribution seems promising. However, we have encountered difficulty with our initial results in modeling snow depth across LVWS with kriging interpolation techniques. We look to improve upon our initial results by modeling the large scale variability of snow depth with binary regression tree methods (Elder 1995, Elder et al., 1997) and modeling small scale variability with kriging techniques. Binary regression trees can more accurately handle abrupt changes in the primary variable, and thus will be used to model snow depth. The estimated snow depths from the binary regression trees will be subtracted from the measured snow depths, and the resulting residuals will be modeled through kriging interpolation. Combining the modeled snow depths and modeled residuals should yield more accurate estimations of the spatial distribution of snow in LVWS.

Acknowledgments

Don Campbell and the other USGS folks from Denver, along with Joe Stock, Eric Allstott, and Doug Bopray provided help with the snow survey. Robin Reich provided tremendous help to modeling efforts. Don Cline, National Operational Hydrologic Remote Sensing Center, NWS, NOAA, coordinated the pre-processing of the aerial photos that were used to construct the 10 m DEM of LVWS. Ralph Root and Larry Fairbank, USGS/BRD, Center for Biological Informatics, provided assistance in constructing the DEM. Meegan Flenniken extended support and editorial wizardry. This research was funded by the Colorado Rockies Global Change Program, U.S. Geological Survey, Loch Vale Watershed Project.

REFERENCES

Bailey, T. C., and A. C. Gatrell, *Interactive Spatial Data Analysis*, Longman Scientific & Technical, Essex, England, 413 pp., 1995.

Baron, J., and M. A. Mast, Regional characterization and setting for the Loch Vale Watershed study, in *Biogeochemistry of a Subalpine Ecosystem: Loch Vale Watershed*, edited by J. Baron, pp. 12-27, Springer-Verlag, New York, 1992.

Breiman, L., J. Friedman, R. Olshen, and C. Stone, *Classification and Regression Trees*, Wadsworth and Brooks, Pacific Grove, CA, 1984.

Caine, N., An elevational control of peak snowpack variability, *Water Resources Bulletin, 11*, 613-621, 1975.

Campbell, D. H., D. W. Clow, G. P. Ingersoll, M. A. Mast, N. E. Spahr, and J. T. Turk, Processes controlling the chemistry of two snowmelt-dominated streams in the Rocky Mountains, *Water Resources Research, 31*, 2811-2821, 1995.

Carroll, S. S., and N. Cressie, A comparison of geostatistical methodologies used to estimate snow water equivalent, *Water Resources Bulletin, 32*, 267-278, 1996.

Chambers, J., and T. Hastie (eds.), *Statistical Models in S*, Wadsworth and Brooks, Pacific Grove, CA, 1992.

Clark, L., and D. Pregibon, Tree-based models, in *Statistical Models in S*, edited by J. Chambers and T. Hastie, pp. 377-419, Wadsworth and Brooks, Pacific Grove, CA, 1992.

Cline, D., *personal communication*, National Operational Hydrologic Remote Sensing Center, NWS, NOAA, Chanhassen, MN, 1997.

Cressie, N. A., *Statistics for Spatial Data*, John Wiley & Sons, New York, 1991.

Doesken, N. J., and A. Judson, *The Snow Booklet: A Guide to the Science, Climatology, and Measurement of Snow in the United States*, Colorado State University Department of Atmospheric Science, Fort Collins, CO, 1996.

Dunlap, L. E., and J. M. Spinazola, Interpolating water-table altitudes in west-central Kansas using kriging techniques, *U. S. Geological Survey Water-Supply Paper 2238*, 1984.

Elder, K., Snow Distribution in Alpine Watersheds, Ph.D. Dissertation, 309 pp., Department of Geography, University of California, Santa Barbara, 1995.

Elder, K., J. Dozier, and J. Michaelsen, Snow accumulation and distribution in an alpine watershed, *Water Resources Research, 27*, 1541-1552, 1991.

Elder, K., W. Rosenthal, and B. Davis, Estimating the spatial distribution of snow water equivalence in a montane watershed, *Proceedings of the Western Snow Conference, 65*, 29-41, 1997.

Frew, J., and J. Dozier, The Image Processing Workbench - portable software for remote sensing instruction and research, *in Proceedings IGARSS '86*, ESA SP-254, pp. 271-276, European Space Agency, Paris, 1986.

Gambolati, G., and G. Volpi, Groundwater contour mapping in Venice by stochastic interpolators, I: theory, *Water Resources Research, 15*, 281-290, 1979.

Herzfeld, U. C., C. S. Lingle, and L. Lee, Geostatistical evaluation of satellite radar altimetry for high-resolution mapping of Lambert Glacier, Antarctica, *Annals of Glaciology, 17*, 77-85, 1990.

Hosang, J., and K. Dettwiler, Evaluation of a water equivalent of snow cover map in a small catchment area using a geostatistical approach, *Hydrological Processes, 5*, 283-290, 1991.

Journel, A. G., and Ch. J. Huijbregts, *Mining Geostatistics*, Academic Press, New York, 1978.

Kneizys, F., E. Shettle, L. Abreu, J. Chetwynd, G. Anderson, W. Gallery, J. Selby, and S. Clough, Users Guide to LOWTRAN7, *Report AFGL-TR-88-0177*, Air Force Geophysics Laboratory, Bedford, MA, 1988.

Logan, L. A., Basin-wide water equivalent estimation from snowpack depth measurements, in *Role of Snow and Ice in Hydrology*, IAHS-AIHS Publ. 107, pp. 864-884, International Association of Hydrological Sciences, Wallingford, UK, 1973.

Matheron, G., Principles of geostatistics, *Economic Geology, 58*, 1246-1266, 1963.

McKay, G. A., and D. M. Gray, The distribution of snowcover, in *Handbook of Snow*, edited by D. M. Gray and D. H. Male, pp. 153-190, Pergamon, New York, 1981.

Megehan, W. F., J. R. Meiman, and B. C. Goodell, Net allwave radiation as an index of natural snowmelt and snowmelt accelerated with albedo reducing materials, *Proceedings of the International Hydrology Symposium*, pp. 149-156, Int. Assoc. of Sci. and Hydrol. et al., Fort Collins, CO, 1967.

Oliver, M., R. Webster, and J. Gerrard, Geostatistics in physical geography. Part I: theory, *Trans. Inst. Br. Geogr., 14*, 259-269, 1989.

Phillips, D. L., J. Dolph, and D. Marks, A comparison of geostatistical procedures for spatial analysis of precipitation in mountainous terrain, *Agricultural and Forest Meteorology, 58*, 119-141, 1992.

Rhea, J. O., and L. O. Grant, Topographic influences on snowfall patterns in mountainous terrain, in *Advanced Concepts and Techniques in the Study of Snow and Ice Resources*, pp. 182-192, National Academy of Sciences, Washington, DC, 1974.

Tabios, G. Q., and J. D. Salas, A comparative analysis of techniques for spatial interpolation of precipitation, *Water Resources Bulletin, 21*, 365-380, 1985.

Wiscombe, W. J., and S. G. Warren, A model for the spectral albedo of snow. I: pure snow, *Journal of the Atmospheric Sciences, 37*, 2712-2733, 1980.

Webster, R., and M. A. Oliver, *Statistical Methods in Soil and Land Resource Survey*, Oxford, New York, 1990.

Zuzel, J., and L. Cox, Relative importance of meteorological variables in snowmelt, *Water Resources Research, 11*, 174-176, 1975.

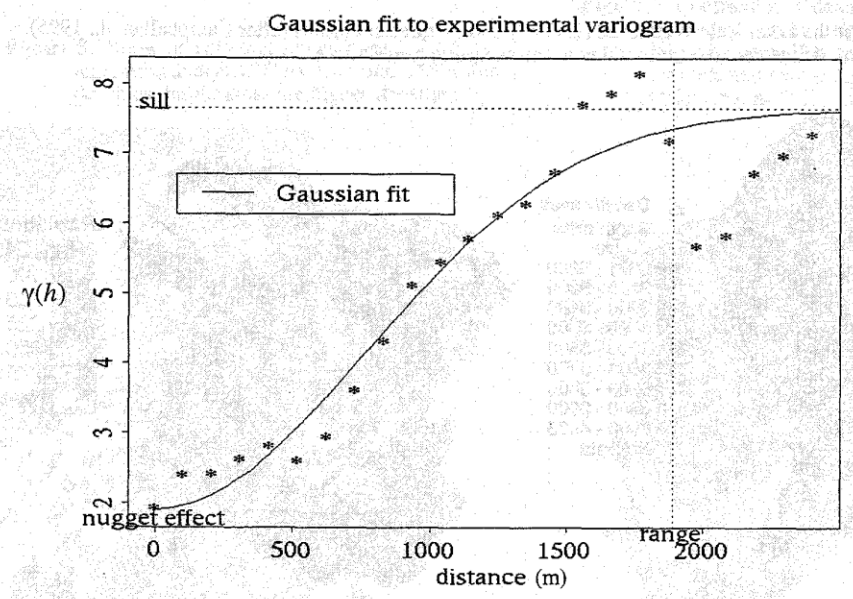

Figure 1. Gaussian fit to the experimental variogram representing the variability of snow depth across LVWS. The nugget effect c_o, the sill c, and the range a are indicated. $\gamma(h)$ is the variogram where h represents the distance class.

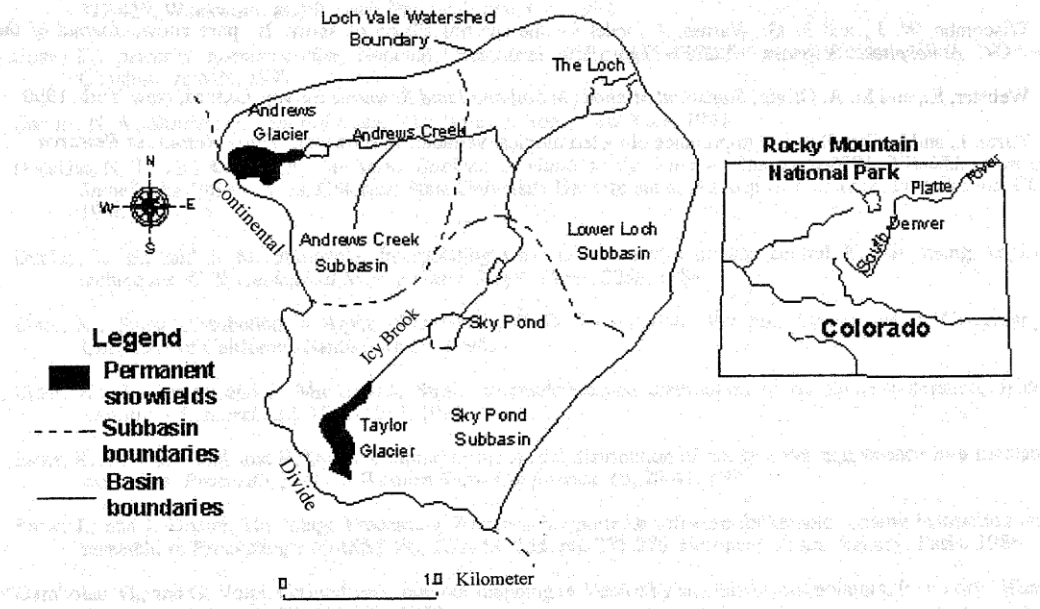

Figure 2. Location of the Loch Vale Watershed (LVWS) and its three subbasins (after Campbell et al., 1995). Subbasins were delineated to correspond with the sampling grid scheme.

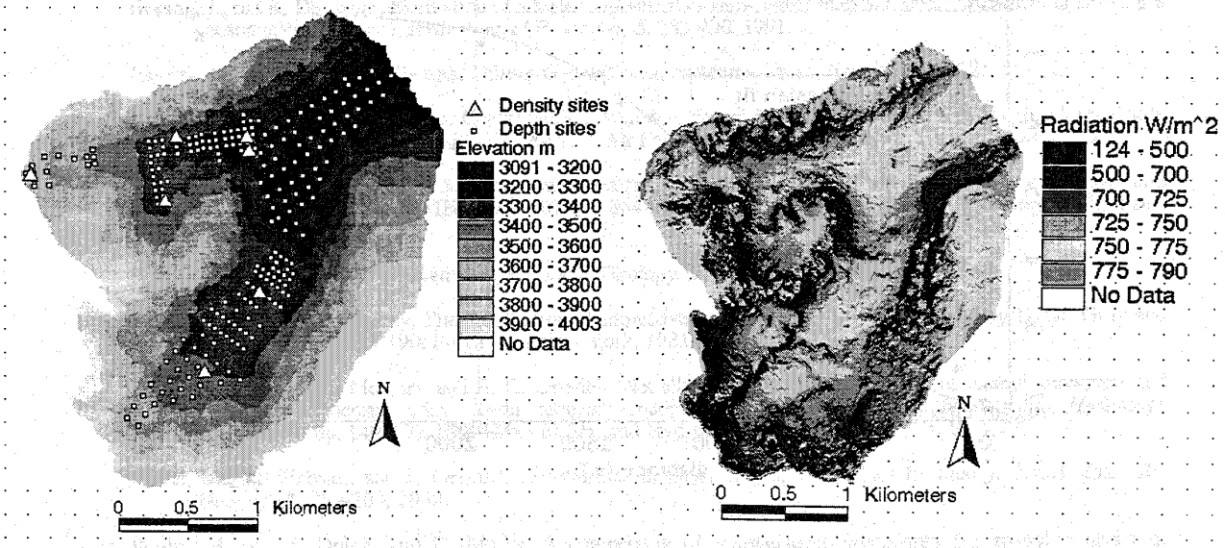

Figure 3. 10 m resolution digital elevation model of LVWS. Dark areas are lower elevations; bright areas are higher elevations. Locations of field measurements of density and depth pinpointed by symbols.

Figure 4. Calculated net solar radiation index over LVWS. Dark areas represent low radiation indices. Bright areas represent high radiation indices.

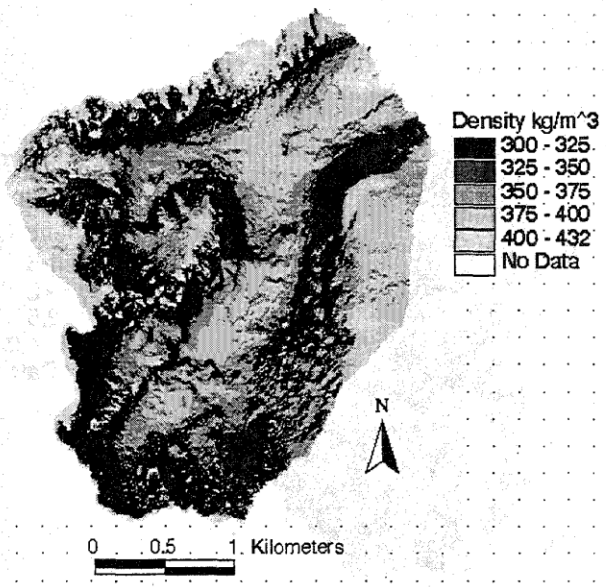

Figure 5. Snow density distributed over LVWS by regression analysis. Dark areas indicate lower densities; bright areas are higher densities.

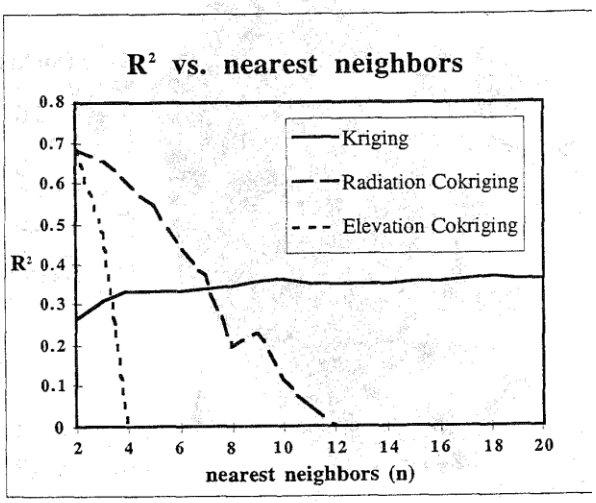

Figure 7. Coefficient of determination (R^2) versus number of nearest neighbors (n) for each kriging model. The optimal n for each model was selected here (Kriging, n=10; Radiation Cokriging, n=2; Elevation Cokriging, n=2).

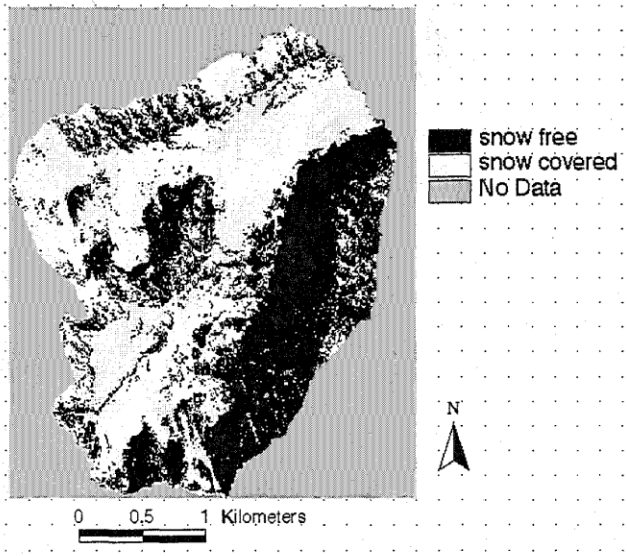

Figure 6. Snow cover map for LVWS. Image was produced using a binary threshold which split the watershed into snow covered areas (white) and snow free areas (black).

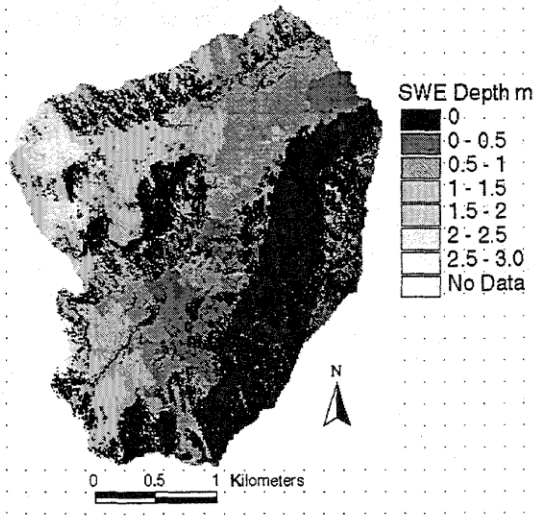

Figure 8. Snow water equivalence map for Kriging model. The modeled depths were combined with the modeled density (Figure 5) and the snow cover map (Figure 6). Dark regions have little or no SWE accumulation; bright areas have higher SWE accumulations.

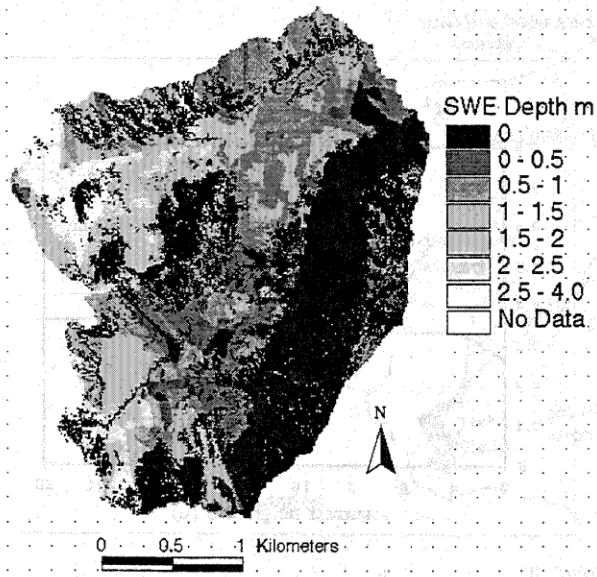

Figure 9. Snow water equivalence map for Radiation Cokriging model. The modeled depths were combined with the modeled density (Figure 5) and the snow cover map (Figure 6). Dark regions have little or no SWE accumulation; bright areas have higher SWE accumulations.

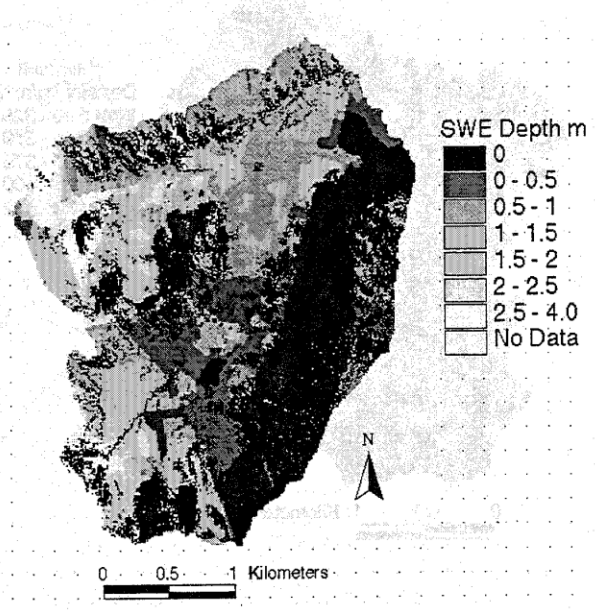

Figure 10. Snow water equivalence map for Elevation Cokriging model. The modeled depths were combined with the modeled density (Figure 5) and the snow cover map (Figure 6). Dark regions have little or no SWE accumulation; bright areas have higher SWE accumulations.